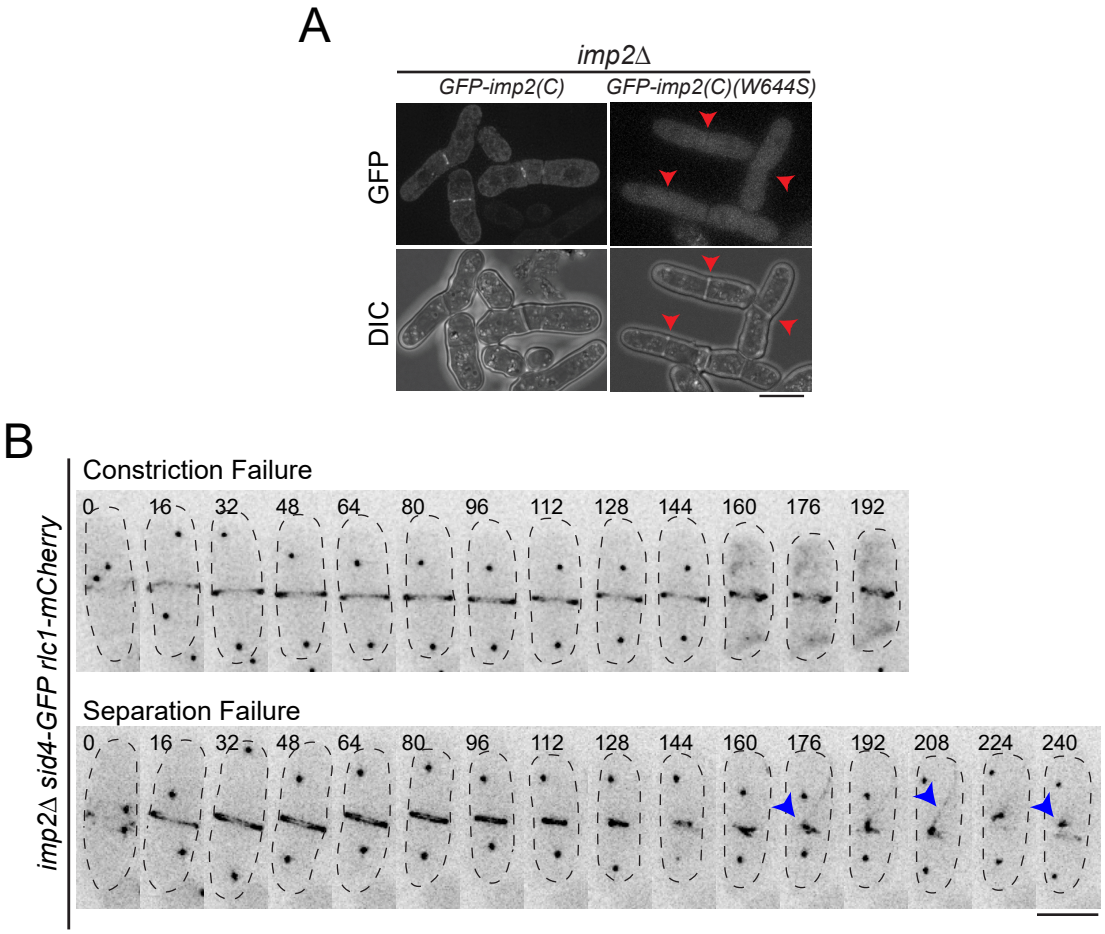

McDonald et al., Figure S1

Figure S1. The Imp2 F-BAR domain is important for cytokinesis, related to Figure 1. A) GFP-Imp2(C) localizes to the contractile ring, while GFP-Imp2(C)(W644S) deficient in SH3 partner binding does not. Red arrowheads indicate division sites lacking GFP-Imp2 signal. Imp2(C) constructs were produced from the *nmt1* promotor in *imp2*Δ cells. Scale bar, 5 µm. B) Representative images of *imp2*Δ *rlc1-GFP sid4-mCherry* cytokinesis defects. Blue arrowhead indicates persistent contractile ring remnants. Scale bar, 5 µm.

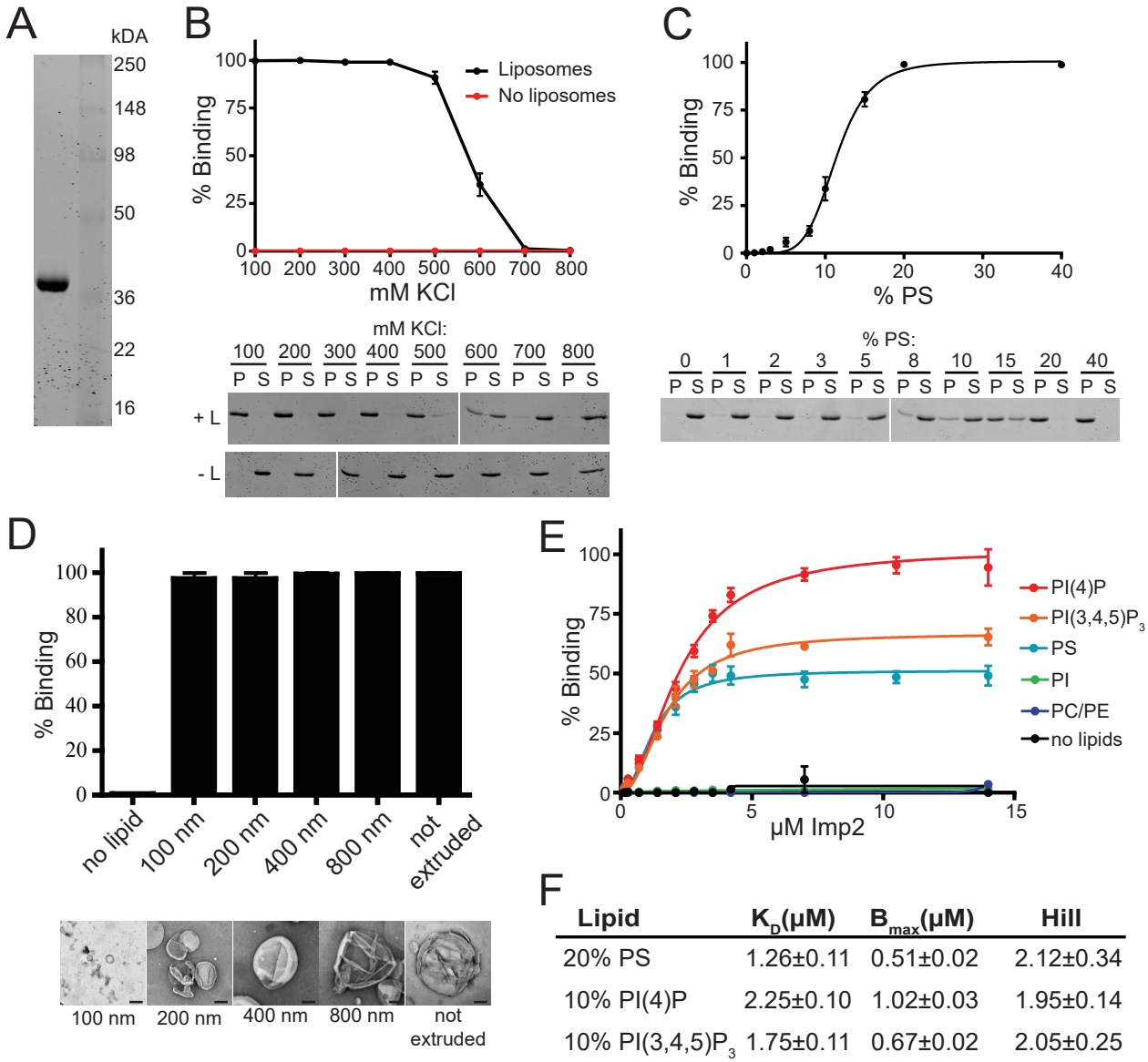

Lipid	K_D(μM)	B_{max}(μM)	Hill
20% PS	1.26±0.11	0.51±0.02	2.12±0.34
10% PI(4)P	2.25±0.10	1.02±0.03	1.95±0.14
10% PI(3,4,5)P_3	1.75±0.11	0.67±0.02	2.05±0.25

McDonald et al., Figure S2

Figure S2. The Imp2 F-BAR domain binds biological membranes, related to Figures 2-3. A) SDS-PAGE and Coomassie Blue stain of purified His_6-Imp2 F-BAR domain. B) Liposome co-pelleting assay between Folch fraction liposomes and the Imp2 F-BAR domain in different concentrations of KCl. P = pellet, bound fraction; S = supernatant, unbound fraction. C) Liposome co-pelleting assay between Imp2 F-BAR domain and liposomes composed of 20% PE, increasing concentrations of PS, and the remainder PC. D) The Imp2 F-BAR domain binds membranes independent of membrane curvature. Top) Quantification of 3 liposome co-pelleting assays between Folch fraction liposomes extruded to the indicated sizes and the Imp2 F-BAR domain. Bottom) Representative negative stain EM images of liposomes extruded to the indicated size. Scale bars, 100 nm. E) Saturation binding assays performed with increasing concentrations of the Imp2 F-BAR domain and liposomes composed of 20% PE, either 20% PS / 10% PI / 10% PI(4)P / 10% $PI(3,4,5)P_3$, and the remainder PC. F) Saturation binding curves from fit with a specific binding model including a Hill slope. The calculated apparent kinetic parameters reflect the affinity of the Imp2 F-BAR domain for liposomes of the indicated compositions. Error bars in all panels indicate SEM from at least 3 experiments.

A

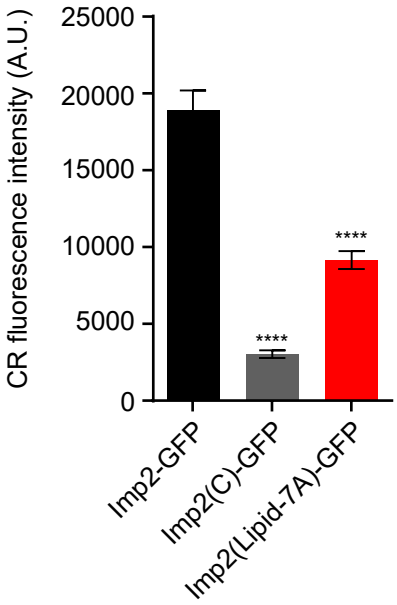

B

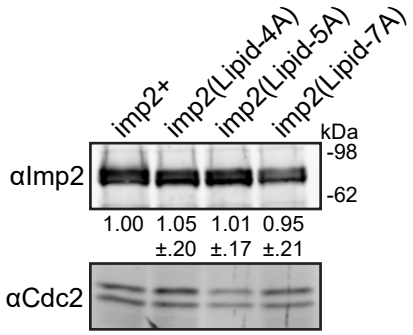

C

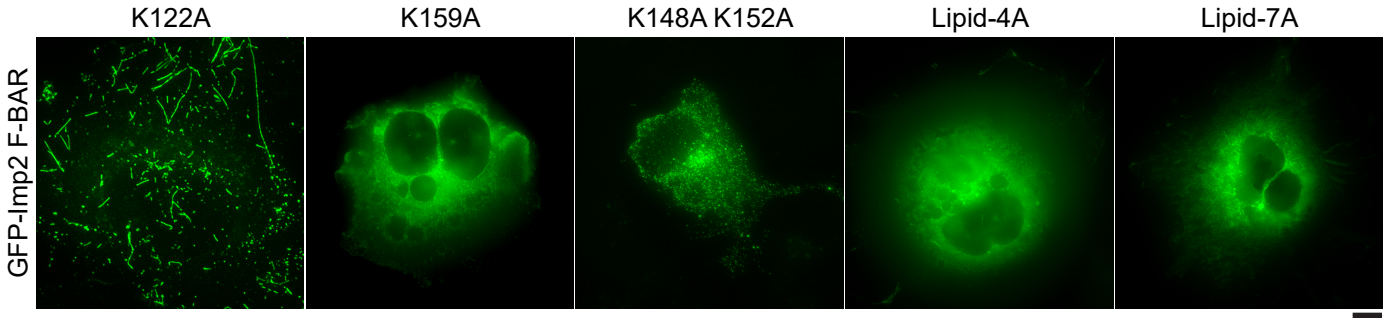

McDonald et al., Figure S3

Figure S3. Imp2 membrane binding mutants, related to Figure 4. A) Fluorescence intensity of the indicated Imp2 mutants at the contractile ring. ****, $p<0.0001$. $n>50$ for each genotype. B) αImp2 western blot for Imp2 protein levels in the indicated strains from Figure 4A. Numbers indicate relative band intensity versus *imp2*$^{+}$ from 3 biological replicates ± SD. C) GFP-Imp2 F-BAR domains with the indicated mutations were expressed in COS-7 cells. Scale bar, 10 µm.

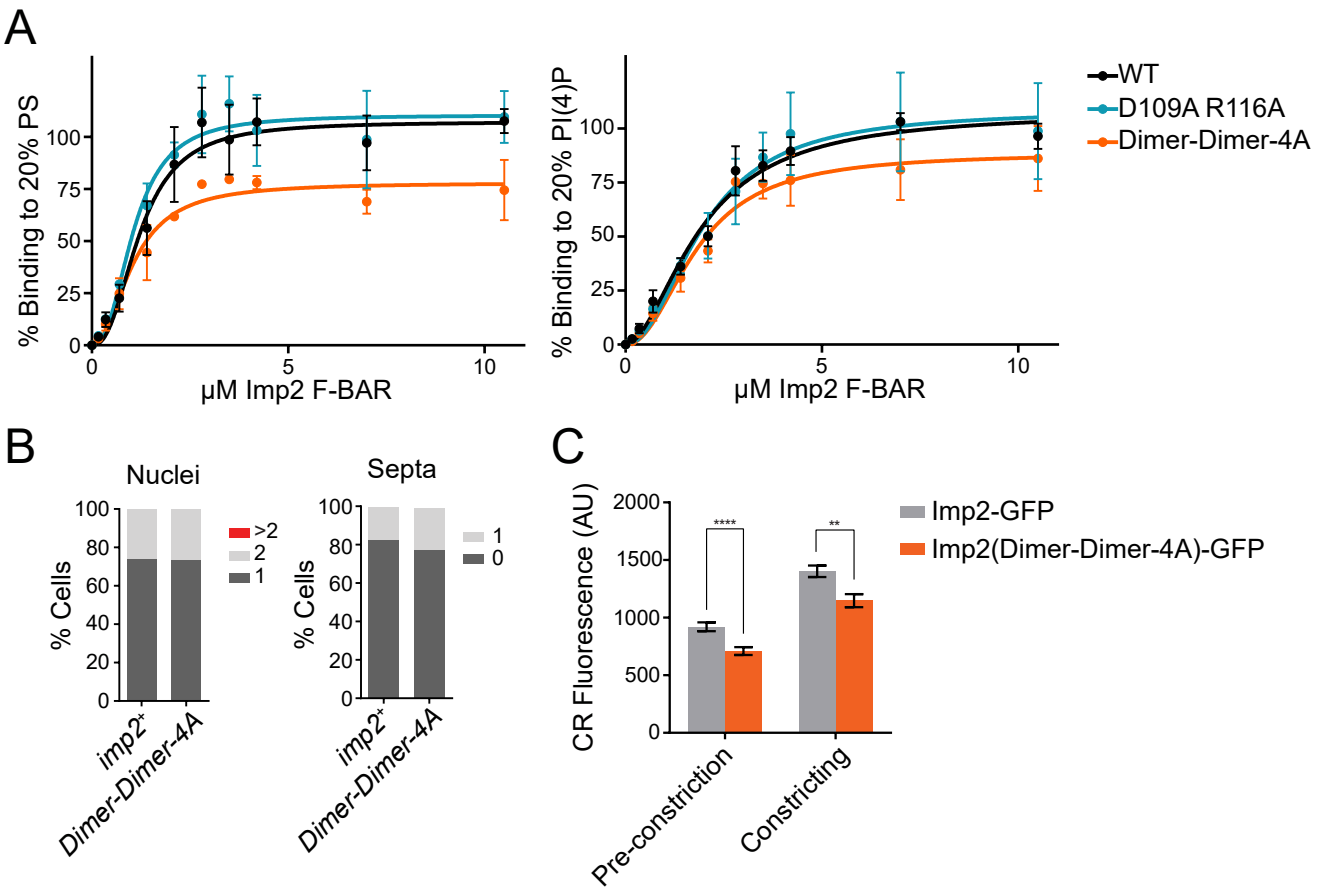

McDonald et al., Figure S4

Figure S4. Imp2 F-BAR domain dimer-dimer mutant properties, related to Figure 6.

A) Liposome binding assays performed between Imp2 F-BAR domain mutants and liposomes composed of 20% PE, either 20% PS / 10% PI / 10% PI(4)P / 10% PI(3,4,5)P_3, and the remainder PC. B) Cytokinesis phenotype quantifications of cells in Figure 8C. n ≥ 300 for each strain. C) Quantification of Imp2-GFP and Imp2(Dimer-Dimer-4A) fluorescence at the contractile ring. n>60 for all conditions. **, p<0.01; ****, p<0.0001. All error bars indicate SEM.

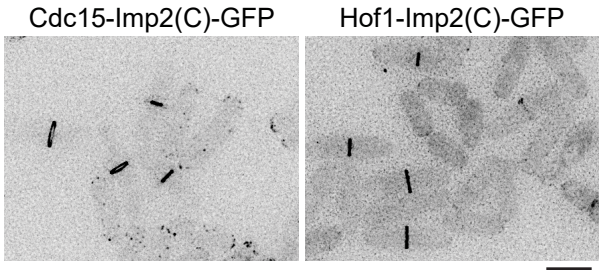

McDonald et al., Figure S5

Figure S5. Both F-BAR fusions are present at the contractile ring, related to Figure 7. Images of the indicated GFP-tagged fusion proteins integrated at the *imp2* locus. Scale bar, 4 µm.

Table S1: Crystallographic data and refinement statistics

	Native	SeMet
Beamline	BM-22	ID-22
Space group	C2	C2
Wavelength	1.0000	0.9792
Unit-cell parameters		
a (Å)	187.34	188.21
b (Å)	33.80	33.79
c (Å)	120.77	121.13
	90.00	90.0
	122.5	122.8
	90.0	90.0
Unique reflections	26635	31323
Completeness (%)	98.5 (88.2)	91.8 (61.3)
Resolution (Å)	20-2.35 (2.43-2.35)	20-2.7 (2.8-2.7)
R_{merge} (%)	9.9 (35.4)	8.9 (20.8)
Redundancy	3.3 (2.5)	2.5 (1.8)
I/σ (I)	11.8 (2.6)	8.2 (3.2)
FOM		0.36

Resolution Limits (Å)	
Number of reflections used in refinement	25302
Number of reflections used to compute R_{free}	1330
R (R_{free})	19.0 (23.9)
# solvent molecules	134
Ramachandran favored	98 %
Ramachandran outlier	0 %
Cβ deviations >0.25Å	0
Bad backbone bonds	0
Bad backbone angles	0
RMS deviation	
Bond, Å	0.003
Angle, º	0.531

Table S2. *S. pombe* strains used in this study.

Figure 1		
KLG246	*ade6-M210 ura4-D18 leu1-32 h$^-$*	lab stock
KLG3462	*imp2::ura4$^+$ ade6-M210 ura4-D18 leu1-32 h$^-$*	lab stock
KLG18636	*imp2(N):KanR ade6-M210 ura4-D18 leu1-32 h$^-$*	this study
KLG15401	*imp2(C):Kan^R ade6-M210 ura4-D18 leu1-32 h$^-$*	this study
KLG14602	*cdc15-140 imp2:Kan^R ade6-M210 ura4-D18 leu1-32 h$^-$*	this study
KLG15507	*imp2(C):Kan^R cdc15-140 ade6-M210 ura4-D18 leu1-32 h$^-$*	this study
KLG14876	*sid4-GFP:Kan^R rlc1-mCherry:Kan^R ade6-M210 ura4-D18 leu1-32 h$^-$*	lab stock
KLG15490	*imp2::ura4$^+$ sid4-GFP:Kan^R rlc1-mCherry:Kan^R ade6-M210 ura4-D18 leu1-32 h$^+$*	this study
KLG17006	*imp2(C):Kan^R sid4-GFP:Kan^R rlc1-mCherry:Kan^R ade6-M210 ura4-D18 leu1-32 h$^-$*	this study
Figure 4		
KLG14575	*imp2(K173A,K177A,K181A,K184):Kan^R ade6-M210 ura4-D18 leu1-32 h$^-$*	this study
KLG17114	*imp2(K159A,K173A,K177A,K181A,K184):Kan^R ade6-M210 ura4-D18 leu1-32 h$^-$*	this study
KLG15449	*imp2(K148A,K152,K159A,K173A,K177A,K181A,K184):Kan^R ade6-M210 ura4-D18 leu1-32 h$^-$*	this study
KLG15489	*imp2(K148A,K152,K159A,K173A,K177A,K181A,K184):Kan^R sid4-GFP:Kan^R rlc1-mCherry:Kan^R ade6-M210 ura4-D18 leu1-32 h$^-$*	this study
KLG14605	*imp2(K173A,K177A,K181A,K184) cdc15-140 ade6-M210 ura4-D18 leu1-32 h$^-$*	this study
KLG17175	*imp2(K159A,K173A,K177A,K181A,K184) cdc15-140 ade6-M210 ura4-D18 leu1-32 h$^-$*	this study
KLG15508	*imp2(K148A,K152A,K159A,K173A,K177A,K181A,K184) cdc15-140 ade6-M210 ura4-D18 leu1-32 h$^-$*	this study
KLG6522	*fic1-GFP:Kan^R ade6-M210 ura4-D18 leu1-32 h$^-$*	lab stock
KLG18130	*imp2(K148A,K152A,K159A,K173A,K177A,K181A,K184) fic1-GFP:Kan^R ade6-M210 ura4-D18 leu1-32 h$^-$*	this study
KLG7420	*spa2-GFP:Kan^R ade6-M210 ura4-D18 leu1-32 h$^+$*	lab stock
KLG18128	*imp2(K148A,K152A,K159A,K173A,K177A,K181A,K184) spa2-GFP:Kan^R ade6-M210 ura4-D18 leu1-32 h$^-$*	this study
KLG4534	*rgf3-GFP:Kan^R ade6-M210 ura4-D18 leu1-32 h$^+$*	lab stock
KLG18127	*imp2(K148A,K152A,K159A,K173A,K177A,K181A,K184) rgf3-GFP:Kan^R ade6-M210 ura4-D18 leu1-32 h$^-$*	this study
Figure 6		
KLG14510	*imp2(D109A,R116A) ade6-M210 ura4-D18 leu1-32 h$^-$*	this study
KLG14505	*imp2(K97A,Q101A,D109A,R116A) ade6-M210 ura4-D18 leu1-32 h$^-$*	this study
KLG14587	*imp2(D109A,R116A) cdc15-140 ade6-M210 ura4-D18 leu1-32 h$^-$*	this study
KLG14601	*imp2(K97A,Q101A,D109A,R116A) cdc15-140 ade6-M210 ura4-D18 leu1-32 h$^-$*	this study
KLG15504	*imp2-3xFLAG:Kan^R ade6-M210 ura4-D18 leu1-32 h$^-$*	lab stock
KLG18081	*imp2(K97A,Q101A,D109A,R116A)-3xFLAG:Kan^R ade6-M210 ura4-D18 leu1-32 h$^-$*	this study
Figure 7		
KLG16951	*cdc15-imp2(C) ade6-M210 ura4-D18 leu1-32 h$^-$*	this study

KLG16949	*hof1-imp2(C) ade6-M210 ura4-D18 leu1-32 h$^-$*	this study
KLG17053	*cdc15-imp2(C) cdc15-140 ade6-M210 ura4-D18 leu1-32 h$^-$*	this study
KLG16950	*hof1-imp2(C) cdc15-140 ade6-M210 ura4-D18 leu1-32 h$^-$*	this study
Figure S1		
KLG15490	*imp2::ura4$^+$ sid4-GFP:Kan^R rlc1-mCherry:Kan^R ade6-M210 ura4-D18 leu1-32 h$^+$*	this study
KLG18635	*imp2(1-320)-GFP:KanR ade6-M210 ura4-D18 leu1-32 h$^-$*	this study
Figure S4		
KLG14500	*imp2(D109A,R116A) sid4-GFP:Kan^R rlc1-mCherry:Kan^R ade6-M210 ura4-D18 leu1-32 h$^-$*	this study
KLG14502	*imp2(K97A,Q101A,D109A,R116A) sid4-GFP:Kan^R rlc1-mCherry:Kan^R ade6-M210 ura4-D18 leu1-32 h$^-$*	this study
KLG7711	*imp2-GFP:Kan^R ade6-M210 ura4-D18 leu1-32 h$^-$*	lab stock
KLG18083	*imp2-GFP(K97A,Q101A,D109A,R116A):Kan^R ade6-M210 ura4-D18 leu1-32 h$^-$*	this study
Figure S5		
KLG18020	*cdc15-imp2(C)-GFP:Kan^R ade6-M210 ura4-D18 leu1-32 h$^-$*	this study
KLG18019	*hof1-imp2(C)-GFP:Kan^R ade6-M210 ura4-D18 leu1-32 h$^-$*	this study

Movie S1. The Imp2 F-BAR domain tubulates giant unilamellar vesicles, related to Figure 5. Unlabeled Imp2 F-BAR domain was added at time 0 to giant unilamellar vesicles composed of 69% DOPC, 15% DOPE, 10% DOPS, 5% PI(4)P, 1% Rhodamine-PE.

Movie S2. Imp2 helical oligomer model, related to Figure 5. Rotation of the Imp2 F-BAR super-helical assembly model from Figure 5H.

Supplemental Experimental Procedures

Molecular biology

The Imp2(C) F-BAR truncation was created in an *imp2* genomic clone (pKLG2332) containing the ORF as well as 500 bp 5' and 3' flanks. Cdc15(1-312) and Hof1(1-294) F-BAR domains were inserted immediately 5' of Imp2(C) for swap experiments. To integrate *imp2* mutants, the entire genomic sequence plus flanks was amplified by PCR and transformed into *imp2::ura4*$^{+}$ cells. Integrants were selected on 5-FOA and confirmed by PCR and sequencing. To visualize the localization of Imp2(C) this sequence was sub-cloned into pREP41GFP. A cDNA fragment encoding Imp2 residues 15-320 was cloned into pET15b for recombinant protein expression. GFP plus an 11 residue linker (-GGGGSGGGGSG-) was cloned into the 5' NdeI site for GFP-F-BAR domain production. cDNA sequences encoding the Imp2 F-BAR domain (residues 15-320) were sub-cloned into pEGFP-C1 (Clontech) for COS-7 cell transfection. Imp2 membrane binding and dimer-dimer mutants were created using a QuickChange Lightning Site-Directed Mutagenesis kit (Agilent Technologies).

Immunoblotting

Imp2 immunoblots were performed with a rabbit polyclonal antibody raised against full length Imp2 protein (Cocalico, Reamstown, PA).

EM image processing

Images of vitrified samples were binned by two to 3.94 Å/pixel, and helixboxer in the EMAN software package (Ludtke et al., 1999) was used to select individual Imp2 tubules with a box width of 260 pixels. The boxed tubules were segmented with 98% overlapped boxes using the Iterative Helical Real Space Reconstruction (IHRSR) program (Egelman, 2007). Tubule sizes between 41 nm and 102 nm of the 30,428 segments

were sorted by diameters. For the reference free 2D class averages, tubules between 54 nm and 64 nm from the 1,777 selected segments in the box size 130 x 130 pixels (7.88 Å/pix) were subjected to 10 rounds of multireference alignment and K-means classification grouping into 20 classed using the SPIDER software package (Frank et al., 1996).

Supplemental References

Egelman, E.H., 2007. The iterative helical real space reconstruction method: Surmounting the problems posed by real polymers. J. Struct. Biol. 157, 83–94.

Frank, J., Radermacher, M., Penczek, P., Zhu, J., Li, Y., Ladjadj, M., Leith, A., 1996. SPIDER and WEB: processing and visualization of images in 3D electron microscopy and related fields. J. Struct. Biol. 116, 190–199.

Ludtke, S.J., Baldwin, P.R., Chiu, W., 1999. EMAN: semiautomated software for high-resolution single-particle reconstructions. J. Struct. Biol. 128, 82–97.